The velocity of aseismic surface deformations between 2016-2020 detected by precise leveling surveys of the Akşehir Simav Fault System in the Bolvadin district, western Anatolia

İbrahim Tiryakioğlu[*,1,2], Kaan Çalışkan[1], Cemal Ozer Yigit[3], Kemal Hastaoğlu[4], Fatih Poyraz[4], Tamer Baybura[1], Eralp Gürlek[1], Çağlar Özkaymak[2,5]

[(1)] Afyon Kocatepe University, Faculty of Engineering, Department of Geomatics Engineering, 03200 Afyon, Turkey

[(2)] Afyon Kocatepe University, Earthquake Research and Implementation Center, 03200 Afyon, Turkey

[(3)] Gebze Technical University, Faculty of Engineering, Department of Geomatics Engineering, 41400, Gebze-Kocaeli, Turkey

[(4)] Cumhuriyet University, Faculty of Engineering, Department of Geomatics Engineering, 58140, Sivas, Turkey

[(5)] Geology Engineering, Faculty of Engineering, Afyon Kocatepe University, TR-3200, Afyonkarahisar, Turkey

Abstract

In this research, the aim was to examine the aseismic surface deformations that occurred in the Bolvadin district center with a precise leveling technique. For this purpose, a geodetic leveling network consisting of eight profiles and 81 benchmarks was installed in the region, and five campaigns of precise leveling measurements were performed between 2016-2020. As a result of the evaluations of the leveling measurements, deformations over time were calculated at each benchmark. In consequence of the evaluation of the five campaign measurements, the deformation amount increased continuously from 2016 to 2020. When the adjusted height differences between 2019-2020 were examined, it was observed that the deformation amount of the previous years doubled. Additionally, deformation rates between −20 and −90 mm/year were estimated using the Kalman filtering methods. According to the current data obtained, the total vertical displacement amount has reached approximately 1 m and the deformation continues today.

1. Introduction

Knowledge of aseismic deformation on active faults has improved greatly over the past few decades because of the implementation of geodetic studies at active tectonics [Tiryakioğlu 2015; Tiryakioğlu et al. 2019; Tiryakioğlu and Bozkus, 2020; Poyraz et al. 2019; Yavasoglu et al. 2020]. Aseismic surface deformations occur as a result of substantial compaction of sediment due to groundwater withdrawal, partly microseismic activity, and tectonic creep [Özkaymak et al., 2019] have been observed in many places for 30 years in Western Anatolian.

The Afyon Akşehir Graben (AAG) representing the southeastern part of the Akşehir-Simav Fault System is one of the important seismological zones in western Anatolia. NW-SE-trending graben is formed by a large number of discontinuous NW-SE and NE-SW-trending active normal fault segments (Figure 1). According to the instrumental and historical earthquake record, many destructive earthquakes have created surface ruptures in AAG [Ambraseys, 1988, 2009; Ambraseys and Jackson, 1998; Tan et al., 2008 Tiryakioğlu et al., 2017; Özkaymak et al., 2019]. The last of these surface faulting earthquakes occurred in 03.02.2002 at 09:11 (Eber) and 11: 26 (Çay) in the south of Bolvadin district with magnitudes of 6.3 and 6.0, respectively (Figure 1).

After the 2002 Çay earthquakes, some progressive aseismic surface deformations began to develop without a destructive earthquake failure in Bolvadin city center on the southwestern part of the NE-SW trending active Bolvadin Fault. In recent studies, linear surface deformations in the Bolvadin settlement area are mapped and studied in terms of their origin and formation [Özkaymak et al., 2015; 2017; 2019; Tiryakioğlu et al., 2017b; 2018;
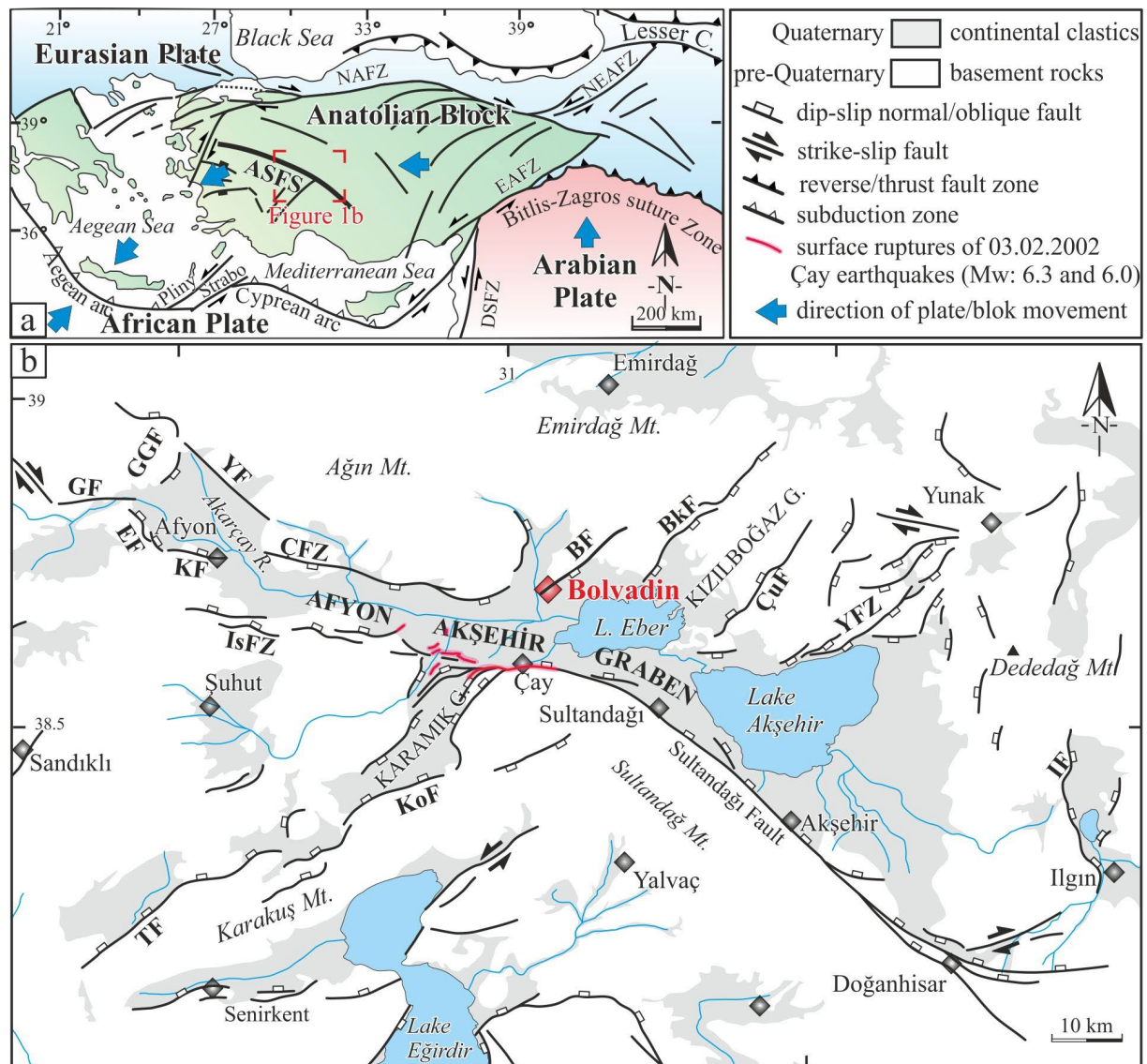

Figure 1. a) Tectonic outline of the eastern Mediterranean area (compiled from Özkaymak, 2015). Abbreviations: ASFS, Akşehir-Simav Fault System; AAG, Afyon-Akşehir Graben; DSFZ, Dead Sea Fault Zone; EAFZ, East Anatolian Fault Zone; NAFZ, North Anatolian Fault Zone; NEAFZ, Northeast Anatolian Fault Zone.
b) The active fault map of the AAG (issued from Özkaymak et al., 2019 and Emre et al., 2011). Abbreviations: KG: Karamık Graben; GF: Gecek Fault; GGF: Gazlıgöl Fault, EF: Erkmen Fault; KF: Karahisar Fault; ÇFZ: Çobanlar Fault Zone; IsFZ: Işıklar Fault Zone; YFZ: Yunak Fault Zone; IF: Ilgın Fault; BF: Bolvadin Fault; BkF: Büyük-Karabag Fault; ÇuF; ÇukurcakFault; YF: Yarıkkaya Fault; KoF: Kocbeyli Fault; TF: Tatarlı Fault.

Imamoglu et al., 2019]. According to these studies, aseismic surface deformations that start on the southwestern side of the Bolvadin City center and can be followed until the northwestern side have been forming since 2002 Çay Earthquakes (Mw:6.0 and 6.3). Trench-based paleoseismological studies indicate that NE-SW trending aseismic surface deformations follow previous linear morphogenic earthquakes on the active Bolvadin Fault. Deformations forming three distinct splays with lengths between 1 and 4 km cause serious damage to urban buildings and infrastructure and have a considerable economic impact in the city center [Özkaymak et al. 2017, Tiryakioğlu et al. 2018a, Tiryakioğlu et al. 2018b, Tiryakioğlu et al. 2019].

Many methods are used to monitor surface deformations, tectonic movements, and surface ruptures that are created after earthquakes [Yıldız et al., 2020; Eyubagil et al., 2021; Aktug et al., 2021; Yavasoglu et al. 2021; Gezgin et al., 2021]. In recent years, studies were carried out to monitor faults with the help of artificial satellite technology. Numerous tectonic studies were completed using continuous or campaign type GNSS observations, synthetic aperture radar (SAR), and satellite images [Tiryakioğlu et al. 2017a, 2018; Ozarpacı et al., 2021; Yalvaç, 2020; Poyraz and Hastaoglu, 2020, Konakoglu, 2021]. One of these methods is the precise leveling method, which is the most accurate and precise geodetic measurement technique to detect elevation changes in millimeter-level [D'Anastasio et al., 2006; Murasea et al., 2013; Hao et al., 2014; Kall et al., 2014; Sabuncu and Ozener, 2014; Poyraz et al., 2019; Tiryakioğlu et al., 2019]. The mean error of the precise leveling method is generallyless than 0.5 mm/√km, which depends on the equipment and methods used. The elevation differences between leveling campaigns performed in different time periods, the amount of subsidence or uplift, andthe deformation ratecan be easily estimated. Therefore, long-term monitoring with the precise leveling technique is required to accurately detect and reveal aseismic surface deformations.

Within the scope of this study, five campaigns of precise leveling measurements (2016-2017-2018-2019-2020) were obtained for aseismic surface deformations occurring in Bolvadin. The velocities of the deformations based on these measurements were calculated by implementing the Kalman filtering method.

2. Field observations on Aseismic Surface Deformations in Bolvadin

In the region between the southern and northeastern parts of Bolvadin settlement, located in the middle of the Afyon-Akşehir Graben, previously unseen surface deformations parallel/semi-parallel to the Bolvadin fault have occurred and continue to occur. In the center of Bolvadin, there are fractures in the garden walls, cracks and crevices in buildings, collapsed sections on roads, and refractions in the underground sewer and water lines due to surface deformations, most of which pass through the residential areas along a line. Along with surface deformations observed in the form of linear cracks and fractures, the block in the southeast of the city center subsided, and the block in the northwest uplifted relatively [Yalçın, 2019; Tiryakioğlu et al., 2019; Çalışkan, 2021].

Several studies were conducted about the origin and formation mechanism of this type of surface deformations observing along the border of the depression areas in western Anatolia [Gürsoy et al., 1997; Demirtaş et al., 2008; Koca et al., 2011; Tiryakioğlu et al., 2015; Tiryakioğlu et al., 2017b; Özkaymak et al., 2017; 2019]. Koca et al. [2011] reported that the aseismic surface deformation on Sarıgöl district has been developing on the surface rupture of 1969 Alasehir Earthquake (Mw:6.9) occurred on Sarıgöl Fault Zone while Özkaymak et al. [2019] reveal that the aseismic surface deformation on Bolvadin district has been developing on the past surface ruptures of active Bolvadin Fault by using trench-based palaeoseismological analyses. The researchers stated that the origin of these deformations was largely caused by consolidation due to the lowering of the groundwater level and partly due to active tectonism in the region. Nevertheless, Imamoglu et al. [2019] reported that the origin of these deformations was exclusively due to the lowering of the groundwater level. Tiryakioğlu and Bozkuş [2020] showed that there is a moderate correlation between groundwater withdrawal and surface deformation in their study. They showed that the deformation process was continued linearly on the Bolvadin fault even in the winter season when there is heavy rainfall. This fault has produced earthquakes in the recent past, and aseismic deformations do not occur in other areas, although there are decreases in groundwater on the other sides of the graben. Aseismic deformations were observed on February 3rd, 2002, after the Çay earthquakes (Mw: 6.3 and 6.0) and provide evidence that surface deformations have tectonic origin along with groundwater levels.

Figure 2. Surface deformations observed in an urban area in Bolvadin.

3. Leveling Network and Measurements

In 2016, a geodetic leveling network was established and leveling measurement was carried out in regions where the surface deformations occurred to examine and monitor the aseismic surface deformations in the Bolvadin district center. In order to monitor the vertical movement occurring northwest and southeast of the NE-SW trending surface deformations, the leveling routes were established to cross the surface deformations perpendicularly. Benchmarks in the leveling network were installed tightly on electricity poles. In this context, a total of eight profiles (leveling routes) consisting of 81 benchmarks were installed (Figure 3-4).
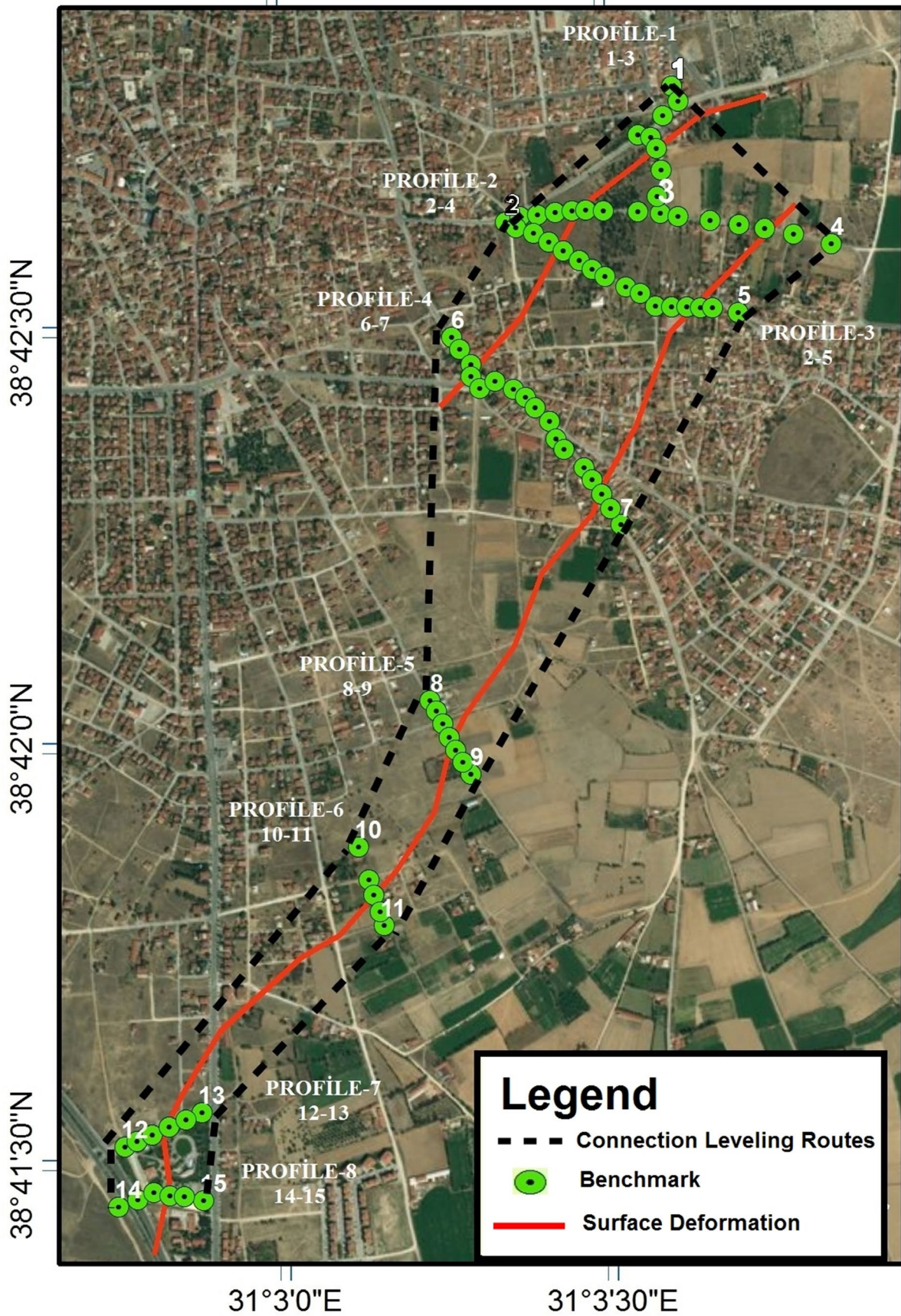
Figure 3. Geodetic leveling network and benchmarks in Bolvadin.

Profile Number	Benchmarks along with the profile
Profile 1	**1**-101-102-103-104-105-106-107-**3**
Profile 2	**2**-201-202-203-204-205-206-207-**3**-301-302-303-304-305-**4**
Profile 3	**2**-401-402-403-404-405-406-407-408-409-410-411-412-413-414-**5**
Profile 4	**6**-501-502-503-504-505-506-507-508-509-510-511-512-513-514-515-**7**
Profile 5	**8**-601-602-603-604-605-**9**
Profile 6	**10**-701-702-703-**11**
Profile 7	**12**-801-802-803-804-**13**
Profile 8	**14**-901-902-903-904-**15**

Table 1. Benchmarks in the Profiles.

Figure 4. A) Installed benchmarks and B) utility poles where the benchmarks were installed.

3.1 Leveling Surveys

In this study, five precise leveling campaigns were conducted to determine the velocities of vertical deformation in the region between 2016 and 2020 (Table 2). The B1-F1-F2-B2 (Backsight1-Foresight1-Foresight2-Backsight1) technique was adopted to carry out precise leveling measurements. The distance between the digital level and leveling staff was constrained to maximum 30 m to meet the conditions of the precise leveling method. During the

measurements, the levels were set so that the observation lines were at least 70 cm above the ground. All of the measurements were made as round-trip, and the starting and ending benchmarks of the established routes were connected by leveling measurements (Table 2).

Number of Campaign	Date of Campaign	Interval with respect to the first campaign
1st	16.08.2016	–
2nd	08.08.2017	12 months
3rd	04.08.2018	24 months
4th	12.07.2019	35 months
5th	22.08.2020	47 months

Table 2. Dates of the Leveling Campaign Measurements.

During the precise leveling route measurements, three repetitions were made for each reading, and the average was taken. If the difference between the same Backsight and Foresight readings was greater than 0.3 mm, the measurements were repeated. While connecting the ending and starting benchmarks of the precise leveling route, the leveling strut and the leveling base plate were used in the measurements. The differences between round-trip measurements on all precise leveling routes did not exceed the tolerance limit calculated from the $4\sqrt{S}$ formula (Table 3). S represents the length of section in kilometers. Since there are no tolerance limit regulations for precision leveling techniques in our country, the tolerance limits and closure errors specified in the German standards (DIN-18710) were adopted in this study (DIN-18710). Moreover, the loop closure errors in the leveling network were checked whether if the systematic errors in the leveling surveys exist or not. Rejection criteria for the loop closure was selected similar to Roelse et al. [1975]. All loop closure errors available in the network were below the maximum error tolerance and similar to Tiryakioğlu et al. [2019].

Profile number	S (m)	Round trip differences (mm)					Maximum acceptable tolerance (mm)	Result
		2016	2017	2018	2019	2020		
1	300	0.8	0.6	0.7	0.1	1	2.1	Accept
2	800	0.8	0.7	0.6	0.5	0.5	3.6	Accept
3	550	0.5	0.4	0.7	0.6	2.7	3.0	Accept
4	600	1.2	0.2	2.4	1	3.1	3.1	Accept
5	250	1.1	1.1	0.1	1	0.9	2.0	Accept
6	150	0.5	1.0	0.1	0.7	0.3	1.5	Accept
7	250	0.5	0.6	0.9	0.5	1.2	2.0	Accept
8	200	0.6	0.2	1.0	0.5	1.4	1.8	Accept

Table 3. Route-based Error Limits.

4. Results and Discussion

Five campaign measurements were separately adjusted by free network adjustment based on the least square error method. The weight of each observation was detected as inversely proportional to the distance of the benchmark interval. The outlier test was performed to detect problematic observations in the network according to the Pope method [Pelzer, 1971, 1985]. Pope test results indicated no outlier observations in the network. Posteriori standard deviations (one sigma) for the five campaigns are given in Table 4.

Campaign	RMSE (mm)
2016	3.40
2017	2.07
2018	2.76
2019	3.11
2020	3.22

Table 4. Posteriori sigma from free network adjustment

S-transformation deformation analysis was performed to statistically detect stable and deformed benchmarks in the leveling network. After detecting stable and deformed benchmarks, the elevation of benchmarks for each campaign was adjusted by the constrained network adjustment method based on benchmark 1, whose stability was proved based on InSAR processing of 18 TerrasarXimages between 2016 and 2020, and conventional deformation analysis. The deformation amount, or changes in height, between two consecutive campaigns, was calculated from the adjusted height of benchmarks. For example, deformation amount between 2019 and 2020 is;

$$\Delta h_{2019}^{2020} = h_{2020} - h_{2019} \tag{1}$$

where, h_{2020} is the adjusted height obtained from the 2020 campaign, h_{2019} is the adjusted height obtained from the 2019 campaign. If Δh_{2019}^{2020} is negative, this indicates subsidence between consecutive periods. If Δh_{2019}^{2020} is positive, it points out an uplift between consecutive periods.

Deformation maps of the region were generated from the deformation amount of benchmarks between 2016 and 2017, 2017 and 2018, 2018 and 2019, 2019 and 2020 (Figure 6). The deformation map was produced based on Kriging interpolation method with linear variogram model by gridding (10 m*10 m).

In the periods 2016-2017, 2017-2018, and 2018-2019, the surface deformation continued, and the maximum deformation amount was approximately −65 mm/year in the southwest of the region (Figure 5). Between 2019-2020, the surface deformation continued but the deformation amount was not similar to that of the previous years; in fact, it was about −95 mm/year in the southwest of the region.

To further investigate the increase in deformation rate over the last two years, we created a time series showing the groundwater levels of a well located in the region from August 2009 to August 2020 (Figure 6). It was observed that the water level of well 28372 had decreased from −16.5 to −19.0 m between August 2009 and August 2015 [Tiryakioğlu and Bozkuş, 2020]. However, the water level of well decreased from −19.0 to −30.30 m between August 2015 and August 2020 (Fig. 6). As seen from the water level measurements, while the water level decrease in 6 years is 2.5 m (0.42 m/year), it is 11.3 m (2.26 m/year) in the last five years. In other words, the rate of the decrease in water
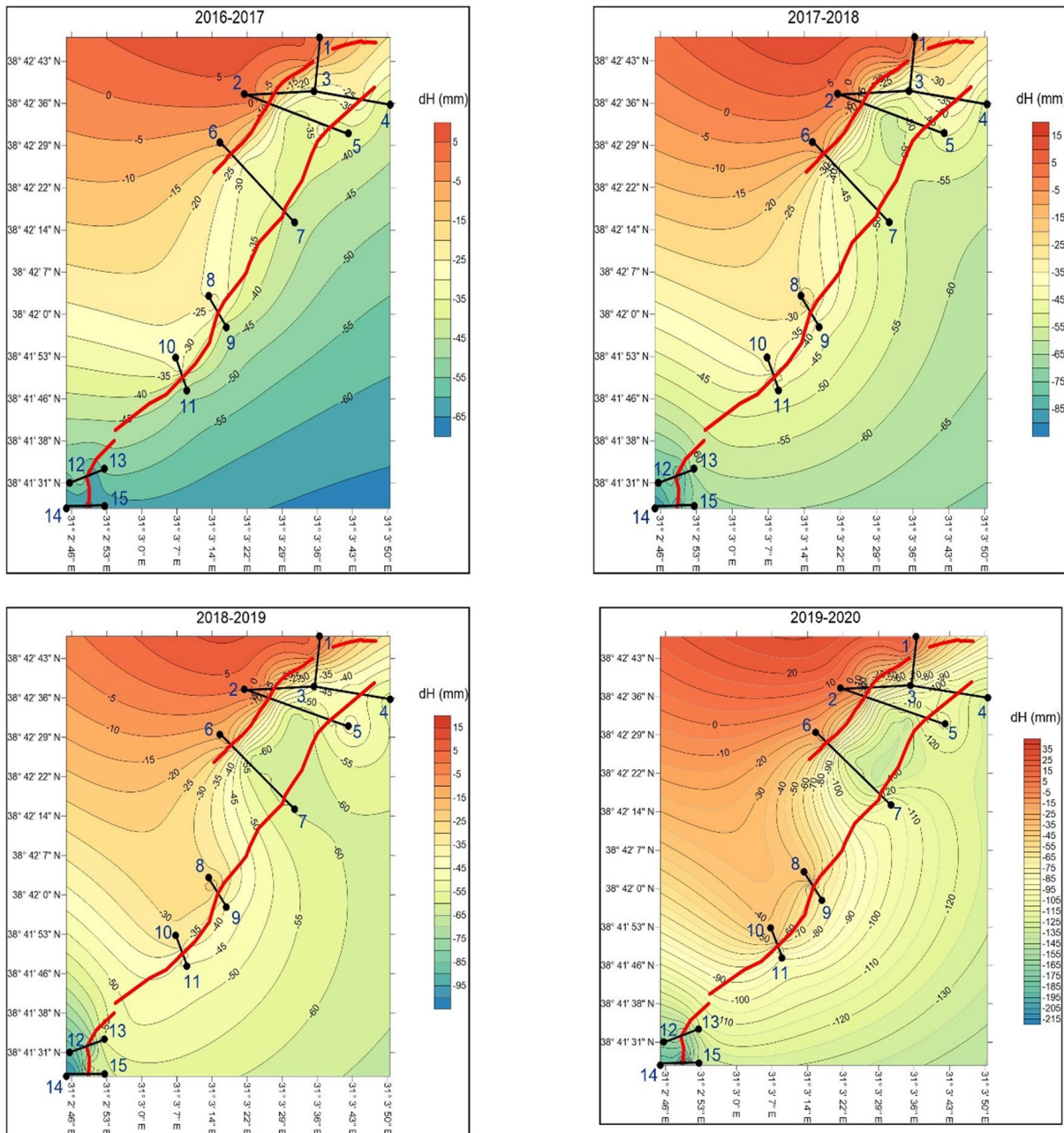
Figure 5. Surface Deformation Maps (Red lines indicate the surface deformation line; black lines indicate the leveling routes/profiles.

level has increased considerably in the last five years. This decrease in the water level is thought to be related to the increase in the amount of deformation in the studied region. Seasonal fluctuations in the water levels occurred in the time series because of intensive agricultural irrigation in the region.

When the elevation changes of benchmarks in the profiles are examined (see Figure 6) one can see the deformation has been constantly increasing from 2016 to 2020. According to these deformation amounts, the velocities of all benchmarks were calculated using the Kalman filtering method.

The reason that the Kalman filtering method was chosen in this situation is that it can determine uniform and irregular movements with a small number of periodic measurements. The purpose of the Kalman filtering method is to calculate the motion parameters in the next period by extrapolating from the motion parameters known in the previous period [Bayrak, 2003]. This model provides an estimation of velocities resulting from deformations. Using the kinematic Kalman model, benchmark movements are defined as a function of time independent of external forces [Hastaoglu, 2013]. In the kinematic single-point model, the benchmarks moving with time at the benchmarks
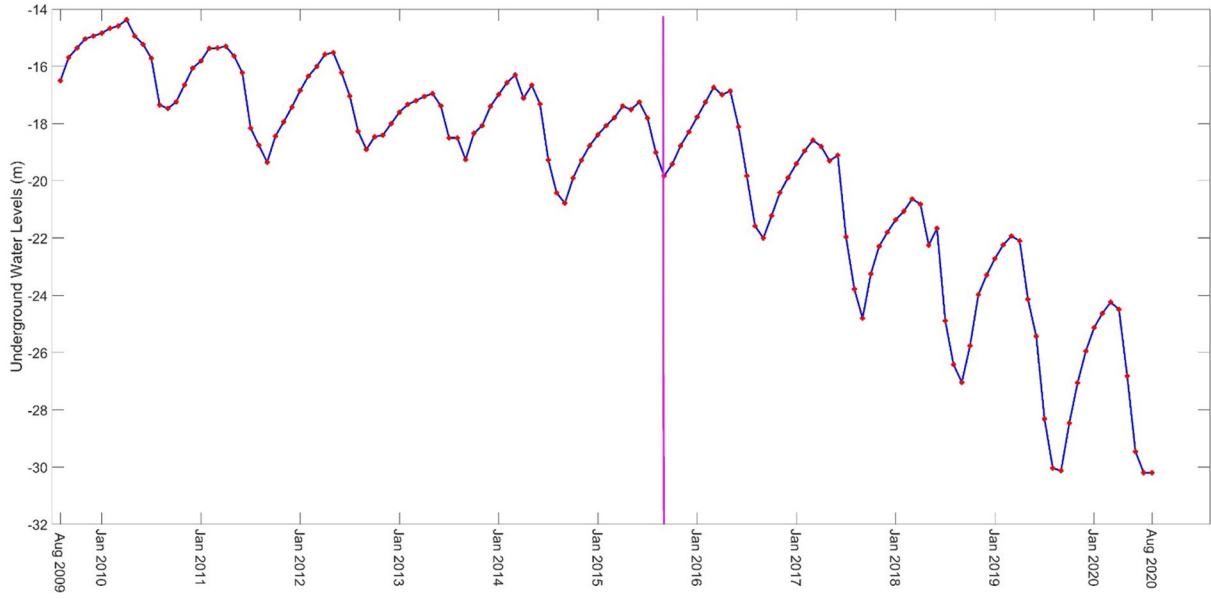
Figure 6. Underground water observation of the well 28372 in the city center of Bolvadin.

of the height network, the magnitude of the movement, and the velocity of the movement are determined by the function in Equation 2 depending on time.

$$H_j^{k+1} = H_j^k + (t_{k+1} - t_k)v_{Hj} \tag{2}$$

In this equation, H_j^{k+1}: the height of point j at time (t_{k+1}) period, H_j^k: the height of point j at time (t_k) period, v_{Hj}: velocities of height of point j, t: measurement time, k = 1,2,…,i (i: measurement period number), j = 1,2,…,n (n number of points). The matrix form of these equations is given in Equations 3 and 4.

$$\bar{Y}_{k+1} = \begin{bmatrix} H \\ v_H \end{bmatrix}_{k+1} = \begin{bmatrix} 1 & (t_{k+1} - t_k) \\ 0 & 1 \end{bmatrix}_{k+1,k} \begin{bmatrix} H \\ v_H \end{bmatrix}_k \tag{3}$$

$$\bar{Y}_{k+1} = T_{k+1,k}\hat{Y}_k \tag{4}$$

$\bar{Y}_{k+1}$: t_{k+1} is the status vector at time t_{k+1}, $\hat{Y}_k$ the status vector at time t_k, and $T_{k+1,k}$ is the prediction matrix. When the noise vector S is added to (3), the prediction and covariance matrix is as follows [Hastaoglu, 2013; Bayrak, 2009; Gülal, 1999].

$$\bar{Y}_{k+1} = T_{k+1,k}\hat{Y}_k + S_{k+1,k}\,w_k \tag{5}$$

$$Q_{\bar{Y}\bar{Y},k+1} = T_{k+1,k}Q_{\hat{Y}\hat{Y},k}\,T_{k+1,k}^T + S_{k+1,k}Q_{ww,k}\,,S_{k+1,k}^T \tag{6}$$

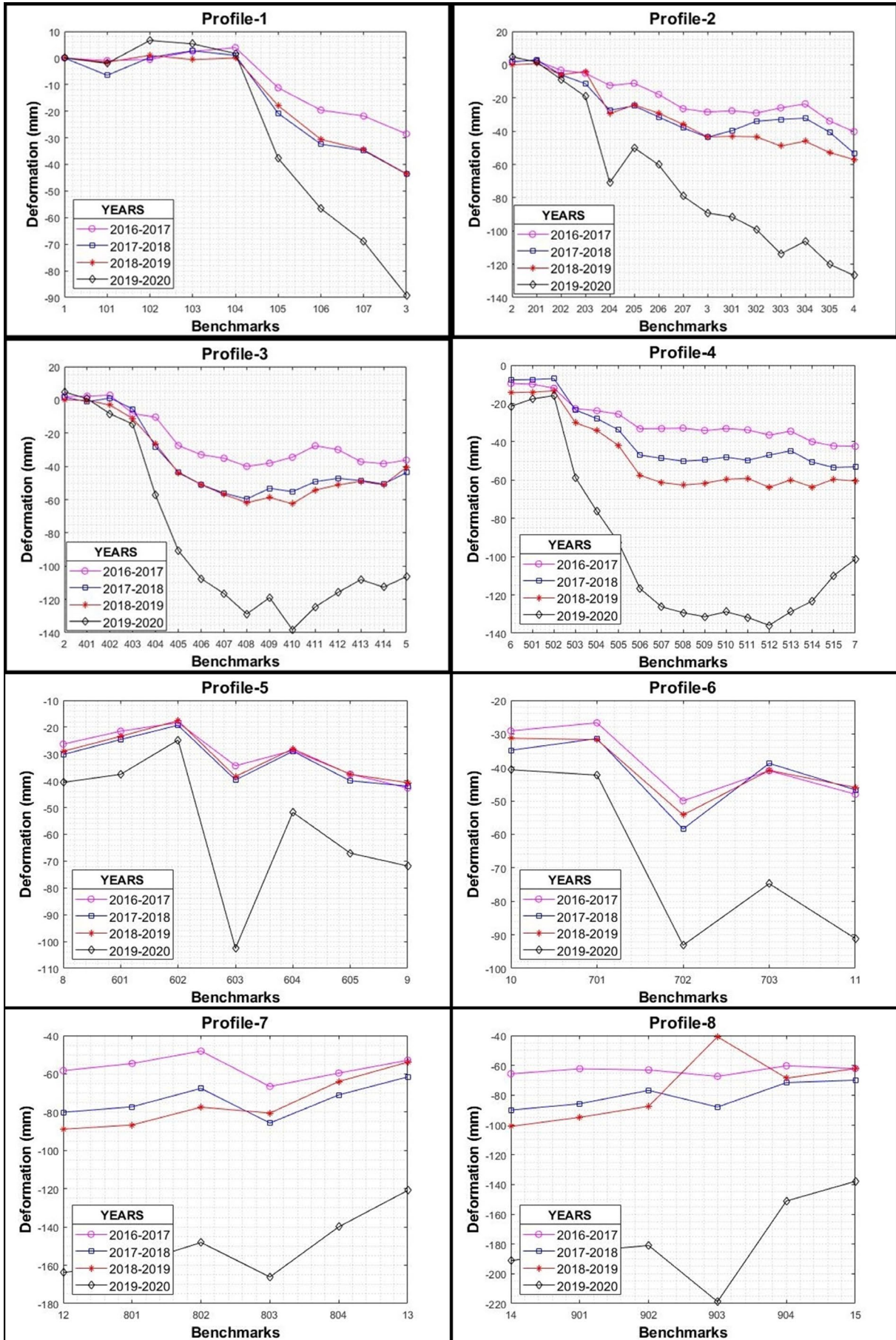$$S_{k+1,k}^T = [(t_{k+1} - t_k) \quad 1] \tag{7}$$

Figure 7. Deformations of the benchmarks in profiles over five years (2016-2020).

$$Q_{ww,k-1} = 4(t_k - t_{k-1})^{-4} Q_{SS,k-1} \qquad (8)$$

$S_{k+1,k}$ is the random noise vector between periods t_{k+1} and t_k. $Q_{\overline{YY},k+1}$, is the cofactor matrix of status vector at time t_k, $Q_{ww,k}$ is the cofactor matrix of system noises at time t_k.

$$l_{k+1} + v_{l,k+1} = A_{k+1}\hat{Y}_{k+1} \qquad (9)$$

l_{k+1}: are measurements at time t_{k+1}, $v_{l,k+1}$ are residuals, A_{k+1} is the coefficient matrix, and $\hat{Y}_{k+1}$: are measurements in period $k+1$.

The prediction and measurement equations of (5) and (9) are combined to form functional and stochastic models for the filter stage as in (10) and (11) [Hastaoglu, 2013; Bayrak, 2009; Acar et al., 2008].

$$\begin{bmatrix} \overline{Y}_{k+1} \\ l_{k+1} \end{bmatrix} = \begin{bmatrix} l \\ A_{k+1} \end{bmatrix} \hat{Y}_{k+1} - \begin{bmatrix} v_{\overline{Y},k+1} \\ v_{l,k+1} \end{bmatrix} \qquad (10)$$

$$Q_i = \begin{bmatrix} Q_{\overline{YY},k+1} & 0 \\ 0 & Q_{ll,k+1} \end{bmatrix} \qquad (11)$$

By solving the model in (10), the movement parameters and their cofactor matrix are calculated.

By using (10) and (11), the annual velocity values of the leveling benchmarks are estimated according to the kinematic Kalman filter model along with their uncertainties (Table 5). In Figure 7, the annual velocity values of the benchmarks are given.

B. No	Velocity (mm/yr)	Sigma (mm/yr)	Test Value	Decision	B. No	Velocity (mm/yr)	Sigma (mm/yr)	Test Value	Decision
1	–	–	–	–	401	0	10.4	0.0	insignificant
2	1.7	9.7	0.2	insignificant	402	−1.7	11.0	0.2	insignificant
3	−48.9	9.9	4.9	significant	403	−9.2	11.5	0.8	insignificant
4	−63.8	12.6	5.1	significant	404	−29.3	12.0	2.5	significant
5	−51.3	13.2	3.9	significant	405	−48.2	12.4	3.9	significant
6	−12.1	13.9	0.9	insignificant	406	−56.5	12.7	4.5	significant
7	−58.7	15.5	3.8	significant	407	−61.8	12.9	4.8	significant
8	−28.6	17.1	1.7	significant	408	−67.3	13.1	5.1	significant
9	−43.5	17.3	2.5	significant	409	−62.1	13.3	4.7	significant
10	−30.6	18.7	1.6	insignificant	410	−66.8	13.4	5.0	significant
11	−49.7	18.8	2.7	significant	411	−58.8	13.4	4.4	significant
12	−82.5	21.1	3.9	significant	412	−56.1	13.4	4.2	significant

B. No	Velocity (mm/yr)	Sigma (mm/yr)	Test Value	Decision	B. No	Velocity (mm/yr)	Sigma (mm/yr)	Test Value	Decision
13	−60.1	20.9	2.9	significant	413	−55.6	13.4	4.2	significant
14	−93.7	21.6	4.3	significant	414	−57.9	13.3	4.4	significant
15	−68.2	21.7	3.1	significant	501	−11.3	14.3	0.8	insignificant
101	−3.1	5.3	0.6	insignificant	502	−10.9	14.6	0.7	insignificant
102	1.7	6.6	0.3	insignificant	503	−30.3	14.9	2.0	significant
103	2.1	7.6	0.3	insignificant	504	−36.1	15.2	2.4	significant
104	1.3	8.3	0.2	insignificant	505	−43.5	15.4	2.8	significant
105	−21.3	8.9	2.4	significant	506	−57.5	15.6	3.7	significant
106	−33.9	9.3	3.6	significant	507	−60.6	15.7	3.9	significant
107	−38.5	9.7	4.0	significant	508	−62	15.8	3.9	significant
201	1.9	10.1	0.2	insignificant	509	−62	15.9	3.9	significant
202	−6	10.3	0.6	insignificant	510	−60.3	15.9	3.8	significant
203	−9.4	10.5	0.9	insignificant	511	−61.3	15.9	3.9	significant
204	−33.2	10.6	3.1	significant	512	−63	15.9	4.0	significant
205	−26.6	10.6	2.5	significant	513	−59.6	15.8	3.8	significant
206	−33.3	10.5	3.2	significant	514	−62.3	15.7	4.0	significant
207	−42.5	10.2	4.2	significant	515	−60	15.6	3.9	significant
301	−47.6	10.6	4.5	significant	601	−24	17.3	1.4	insignificant
302	−47.4	11.1	4.3	significant	602	−18	17.4	1.0	insignificant
303	−50.7	11.6	4.4	significant	603	−46.3	17.4	2.7	significant
304	−47.7	12.0	4.0	significant	604	−30.2	17.4	1.7	significant
305	−56.5	12.3	4.6	significant	605	−40.3	17.4	2.3	significant
801	−79.8	21.2	3.8	significant	701	−29.5	18.8	1.6	insignificant
802	−71.7	21.2	3.4	significant	702	−56.1	18.9	3.0	significant
803	−83.6	21.1	4.0	significant	703	−42	18.8	2.2	significant
804	−69.6	21.0	3.3	significant	903	−81.8	21.8	3.8	significant
901	−89.2	21.7	4.1	significant	904	−72.2	21.8	3.3	significant
902	−84	21.8	3.9	significant					

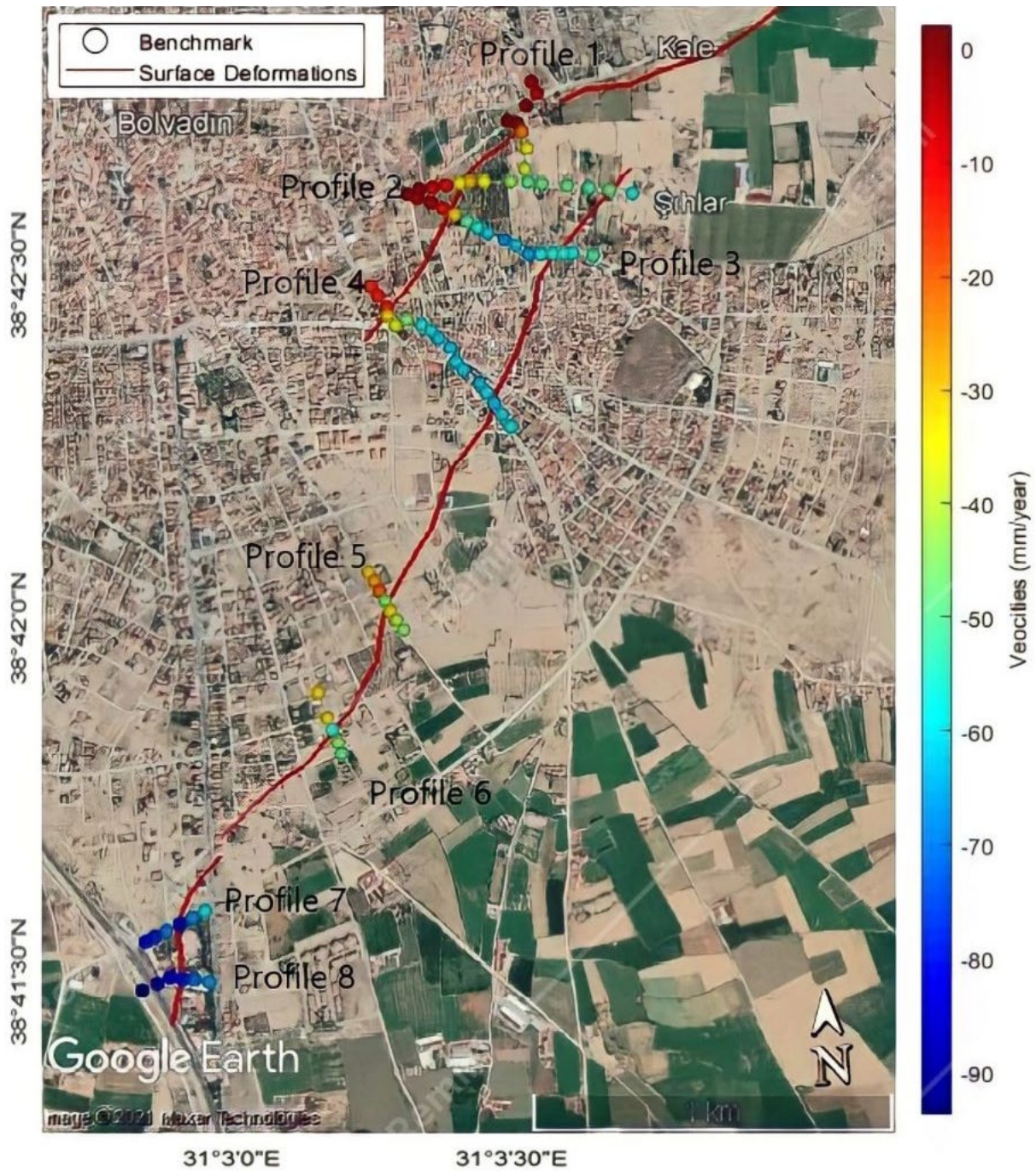**Table 5.** Velocity values of benchmarksestimated from Kalman filtering.

Figure 8. Deformation rate (velocity).

When Table 5 and Figure 8 are examined, especially at the benchmarks in profile 7 (between12 and 13) and profile 8 (between 14 and 15) in the southern region, the subsidence values in the west-east direction vary between approximately 9 cm/yr and 7 cm/yr. These subsidence values decrease as one goes to the north and vary between 3 cm/yr and 5 cm/yr in profile 5 (between 8 and 9) and profile 6 (between 10 and 11). In profile 2 (between 2 and 4), 3 (between 2 and 5), and 4 (between 6 and 7), the subsidence values increase in the west-east direction and vary between 1 cm/year and 6 cm/year. In profile 1 (between 1 and 3), the subsidence values were determined as 1-4 cm/yr in the north-south direction. In general, an increase is observed in the subsidence values in the southeast direction in the study area.

5. Conclusion

In recent years, buildings close to active faults in Western Anatolia have been experiencing bending and cracking because of aseismic deformation activity, although no earthquake has occurred yet. The most prominent examples of this type of deformation in western Anatolia were observed in the settlement areas of Sarıgöl to the east of the Gediz graben and Bolvadin located in the middle part of the Afyon Akşehir graben. These deformations occur on the surface rupture formed after the 1969 Alaşehir earthquake (M:6.9) in the Sarıgöl settlement area and on the southwestern continuation of the Bolvadin fault in the region where the 2002 Çay earthquakes (Mw:6.3 and 6.0) occurred in the Bolvadin settlement area.

In this study, an 81-benchmarks leveling network was established to determine the surface deformations, and 5 campaigns of measurements were conducted between 2016 and 2020. These leveling lines consisted of eight profiles vertical to the deformations. As a result of the evaluations of the leveling measurements, deformations were calculated at each benchmark. It was observed that while the annual velocities were −1.5-5.5 cm/yr along all profiles between 2016 and 2019, it reached −5, −12 cm/yr approximately between 2019-2020. The velocities of the previous years doubled in this period. Deformation rates between −20 and −90 mm/yr were estimated using the Kalman filtering methods in all periods. However, there was a decrease in the groundwater level due to intensive agricultural irrigation in the study area. It is stated in many international studies that deformations in the form of aseismic surface faulting occur along faults in the region with the compaction of unconsolidated or less consolidated alluvial sediments due to the decrease in the groundwater level [Holzer, 1980, 1984, Imamoğlu et al 2019, Özkaymak et al. 2017]. Since the investigated region is settlement area and tectonically active, 3 continuous GNSS monitoring stations have been established in addition to the leveling network to monitor the region.

References

Acar, M., T. Ozludemir, S. Erol, R.N. Celik, and T. Ayan (2008). Kinematic landslide monitoring with Kalman filtering, Nat. Hazards Earth Syst. Sci., 8, 213-221.

Aktuğ, B., I. Tiryakioğlu, H. Sözbilir, H. Özener, Ç. Özkaymak, C.O. Yiğit, H.İ. Solak, E.E. Eyübagil, B. Gelin, O. Tatar and M. Softa (2021). GPS derived finite source mechanism of the 30 October 2020 Samos Earthquake, Mw=6.9 in Aegean extensional region, Turkish J. Earth Sci., 30, 718-737.

Ambraseys, N.N. and J. A. Jackson (1998). Faulting associated with historical and recent earthquakes in the Eastern Mediterranean region. Geophys J. Int., 133, 390-406.

Ambraseys, N.N. (1988). Temporary seismic quiescence: SE Turkey, Geophys J., 96, 311-331.

Ambraseys N.N. (2009). Earthquakes in the Mediterranean and Middle East: a multidisciplinary study of seismicity up to 1900, Cambridge University Press, 947.

Bayrak, T. (2003). Developing a dynamic deformation model and a dynamic movement surface model for landslides. PhD, Karadeniz Technical University, Graduate School of Natural and Applied Sciences, Trabzon, Turkey, 140, (in Turkish).

Bayrak, T. (2009). Determining the influence of rainfall on the activity of Kulugun landslide, Fresenius Environ. Bull., 18, 1249-1255.

Çalışkan, K. (2021). The determination of vertical deformation velocities in the city center of Bolvadin/Afyonkarahisar, Graduate School of Natural and Applied Sciences, Afyon Kocatepe University, M.Sc. Thesis, Afyonkarahisar, Turkey, 81, (in Turkish).

D'Anastasio E., P.M. De Martini, G. Selvaggi, D. Pantosti, A. Marchioni and R Maseroli (2006). Short-term vertical velocity field in the Apennines (Italy) revealed by geodetic levelling data, Tectonophys., 418, 219-234.

Demirtaş, R., Yavuz, M.A. ve Şahin, B. (2008). Manisa ili, Sarıgöl ilçesi imar planı sınırları içerisinde geçen gediz çöküntüsüne ait fay zonunun Paleosismolojik ve Yüzey Faylanması Tehlike Zonuaçısından Değerlendirilmesi. Afet İşleri Genel Müdürlüğü Raporu, 17s, (In Turkish unpublished).

DIN 18710-4 (2010). Engineering survey – Part 4: Deformation measurements, Deutsches Institut fur Normung E.V., (DIN), 31, Germany.

Emre, Ö., T.Y. Duman, S. Özalp, Ş. Olgun, and H. Elmacı (2011). 1:250.000 scale active fault map series of Turkey, İzmir (NJ 35-7) Quadrangle, Serial number: 6, General Directorate of Mineral Research and Exploration, Ankara, Turkey.

Emre, Ö., T.Y. Duman, S. Özalp, Ş. Olgun, H. Elmacı F. Şaroğlu, Olgun, Ş. And T. Çan (2018). Active fault database of Turkey, Bull. Earthq. Eng., 16, 8, 3229-3275.

Eyübagil, E.E., H.İ. Solak, U.S. Kavak, İ. Tiryakioğlu, H. Sözbilir, B. Aktuğ and Ç., Özkaymak (2021). Present-Day strike-slip deformation within the southern part of İzmir Balıkesir Transfer Zone Based on GNSS Data And implications for seismic hazard assessment, Western Anatolia, Turkish J Earth Sci., 30, 143-160

Gülal, E. (1999). Kalman filtreleme tekniğininde formasyon ölçülerinin analizinde uygulanmasıì, Journal of Yıldız Technical University 1, 10-19, (in Turkish).

Gürsoy H, Temiz H, Tatar O, Barka A (1997). Gediz grabeni güney kenarındaki güncel deformasyon verileri, II. İzmir ve ÇevresininJ eoteknik ve Deprem Sorunları Sempozyumu, Bildiri Özetleri, İzmir, Turkey, 14, (in Turkish).

Hao M., Q. Wang, Z. Shen, D. Cui, L. Ji, Y. Li and S. Qin (2014). Present day crustal vertical movement inferred from precise levelling data in eastern margin of Tibetan Plateau, Tectonophys., 632, 281-292.

Hastaoglu K.O. (2013). Investigation of the groundwater effect on slow-motion landslides by using dynamic Kalman filtering method with GPS: Koyulhisar town center, Turk, J. Earth Sci., 22, 6, 1033-1046.

Imamoglu, M., F. Kahraman, Z. Cakir, and F. Balik-Sanli (2019). Ground deformation analysis of Bolvadin (W. Turkey) by means of Multi-Temporal InSAR Techniques and Sentinel-1 data, Remote Sens., 11, 1069.

Kall T., T. Oja, and K. Tänavsuu (2014). Postglaciall and uplift in Estonia based on four precise levellings, Tectonophys., 610, 25-38.

Koca, M. Y., H. Sözbilir, ve B. Uzel (2011). Sarıgöl Fay Zonu Boyunca Meydana Gelen Deformasyonların Nedenleri Üzerine bir araştırma. Jeoloji Mühendisliği Dergisi, 35, 2, 151-173, (InTurkish).

Konakoglu, B. (2021). Prediction of geodetic point velocity using MLPNN, GRNN, and RBFNN models: a comparative study, Acta Geod. Geophys., 56, 2, 271-291.

Murasea M., N. Matta, C.H. Lin, W.S. Chen and N. Koizumie (2013). An episodic creep slip event detected by a precise levelling surveys at the central part of the Longitudinal Valley Fault, eastern Taiwan, Tectonophys., 608, 904-913.

Oktar, O., H. Erdoğan, F. Poyraz and I. Tiryakioğlu (2022). Investigation of deformations with the GNSS and PSInSAR methods, Arab. J. Geosci. 15, 8.

Özarpacı, S., U. Doğan, S. Ergintav, Z. Çakır, A. Özdemir, M. Floyd and R. Reilinger (2021). Present GPS Velocity Field Along 1999 Izmit Rupture Zone: Evidence for Continuing After slip 20 Years After the Earthquake, Geophys. J. Int., 224, 3, 2016-2027.

Özkaymak, Ç. (2015). Tectonic analysis of the Honaz fault (western Anatolia) using geomorphic indices and the regional implications, Geodinamica Acta, 27, 110-129.

Özkaymak, Ç., H. Sözbilir , İ. Tiryakioğlu and T. Baybura (2017). Geologic, geomorphologic and geodetic analyses of surface deformations observed in Bolvadin (Afyon - Akşehir Graben, Afyon), Geol. Bull. Turkey, 60, 169-188.

Özkaymak Ç., H. Sözbilir, M. Gecievi and I. Tiryakioğlu (2019). Late Holocene coseismic rupture and aseismic creep on the Bolvadin Fault, AfyonAkşehir Graben, western Anatolia, Turk. J. Earth Sci., 28, 787-804.

Pelzer, H. (1971). For the analysis of geodetic deformation measurements (in German), Deutsche Geodätische Kommission, München, 164.

Pelzer, H. (1985). Grundlagen der mathematischen Statistik und der Ausgleichsrechnung, in: GeodätischeNetze in Landes- und Ingenieurvermessung II, edited by Pelzer, H. Konrad Wittwer, Stuttgart, 3-120.

Poyraz, F. and K.Ö. Hastaoğlu, (2020). Monitoring of tectonic movements of the Gediz Graben by the PSInSAR method and validation with GNSS results, Arab. J. Geosci., 13, 844.

Poyraz, F., K.O. Hastaoğlu, F. Koçbulut, İ. Tiryakioğlu, O. Tatar, M. Demirel, H. Duman, C. Aydın, A.F. Ciğer, O. Gursoy, T. Turk and R. Sığırcı, (2019). Determination of the Block Movements in the eastern Section of the Gediz Graben (Turkey) from GNSS measurements, J. Geodyn., 123, 38-48.

Roelse A., H.W. Granger, and J.W. Graham (1975). The adjustment of the Australian levelling survey 1970 - 1971, second edition, Technical Report 12, Division of National Mapping, Canberra.

Sabuncu A. and H. Ozener (2014). Monitoring vertical displacements by precise levelling: a case study along the Tuzla Fault, Izmir, Turkey, Geomat. Nat. Haz. Risk, 5, 320-333.

Tan, O., M.C. Tapırdamaz and A. Yoruk (2008). The earthquake catalogues for Turkey, Turk. J. Earth Sci., 17, 405-418

Tiryakioğlu, I. (2015). Geodetic aspects of the 19 May 2011 Simav Earthquake in Turkey, Geomat. Nat. Hazards Risk., 6, 1, 76-89.

Tiryakioğlu, I., C.O. Yiğit, H. Yavaşoğlu, M.H. Saka, and R.M. Alkan, (2017a). The Determination of interseismic, coseismic and postseismic deformations caused by the Gökçeada-Samothraki Earthquake (2014, Mw: 6.9) Based On GNSS Data, J. African Earth Sci., 133, 86-94.

Tiryakioğlu, İ., Ç. Özkaymak, M. Yaçın, T. Baybura, M. Yılmaz, M.A. Uğur, C.O. Yiğit A.A. Dindar, F. Poyraz, M. Uysal, H. Sözbilir and E. Gülal, (2017b). Monitoring the current tectonic Movements in Aksehir-Simav Fault System: Levelling Studies 4, Uluslararası Deprem Mühendisliği ve Sismoloji Konferansı, 11-13 Ekim 2017 - Eskişehir/ Türkiye, (In Turkish).

Tiryakioğlu, İ., Ç. Özkaymak, T. Baybura, H. Sözbilir and M. Uysal (2018a). Comparison of Palaeostress Analysis, Geodetic Strain Rates and Seismic Data in the Western Part of The Sultandağı Fault in Turkey, Ann. Geophys., 61, 3, 1-14.

Tiryakioğlu, I., M.A. Uğur, and Ç. Özkaymak (2018b). Determination of Surface Deformations with Global Navigation Satellite System Time Series, 20th International Research conference on Earth Sciences, Technologies and Applications, 351-354, 3-4, Amsterdam, Netherlands.

Tiryakioğlu, İ., C.O. Yiğit Ç. Özkaymak, T. Baybura, M. Yılmaz, M.A. Uğur, M. Yalçın. F. Poyraz, H. Sözbilir, and E. Gülal (2019). Active Surface Deformations Detected By Precise Levelling Surveys In The Afyon-Akşehir Graben, Western Anatolia, Turkey GEOFIZIKA, 36, 1, 33-52.

Tiryakioğlu, İ. and H.B. Bozkuş (2020). Determination of Surface Deformations in Bolvadin Fault by the Precision Leveling Method and Investigation of the Relationship with Underground Water, Boll. Geofis. Teor. Appl., 61, 4, 499-516.

Yalçın M, (2019). The Monitoring Of Bolvadin Fault Crust Deformation With Precise Levelling, Afyon Kocatepe University, Graduate School of Natural and Applied Sciences, M.Sc. Thesis, 54, Afyonkarahisar.

Yavasoglu, H.H., I. Tiryakioğlu, M.F. Karabulut, E.E. Eyübagil, A. Ozkan, F. Masson, E. Klein, V.E. Gulal, R.M. Alkan, M.N. Alkan, M. Isiler and A.E. Arslan, (2021). New Geodetic Constraints to Reveal Seismic Potential of Central Marmara Region, Turkey, Boll. Geofis. Teor. Appl., 62, 3, 513-526.

Yalvac, S. (2020). Validating InSAR-SBAS results by means of different GNSS analysis techniques in medium- and high-grade deformation areas, Environ, Monit. Assess., 192, 120.

Yıldız, S.S., A. Özkan, H.H. Yavaşoğlu, F. Masson, İ. Tiryakioğlu, M.N. Alkan, and S. Bilgi, (2020). Determination of recent tectonic deformations in the vicinity of Adana-Osmaniye-Hatay-Gaziantep triple junction region by half-space modeling, Comptes Rendus Geosci., 35, 3, 225-234.

Yavaşoğlu, H.H., M.N. Alkan, S. Bilgi and Ö. Alkan, (2020). Monitoring aseismic creep trends in the İsmetpaşa and Destek segments throughout the North Anatolian Fault (NAF) with a large-scale GPS network Geosci. Instrum. Method. Data Syst., 9, 1, 25-40.

*CORRESPONDING AUTHOR: İbrahim TIRYAKIOĞLU,

ANS Campus, Department of Geomatics Engineering, Engineering Faculty, Afyon Kocatepe University u.tr, 03200. Afyon, Turkey, e-mail: itiryakioğlu@aku.edu.tr